Combustion, Explosion, and Shock Waves, Vol. 41, No. 6, pp. 727–744, 2005

Soot Formation in Combustion Processes (Review)

Z. A. Mansurov[1]

UDC 536.46

Translated from *Fizika Goreniya i Vzryva*, Vol. 41, No. 6, pp. 137–156, November–December, 2005.
Original article submitted April 19, 2005.

A review is given of recent papers on the phenomenology, kinetics, and mechanism of soot formation in hydrocarbon combustion; the effects of various factors on the formation of polycyclic aromatic hydrocarbons, fullerenes, and soot, low-temperature soot formation in cool flames, combustion in electric field, and the paramagnetism of soot particles from an ecological viewpoint are considered.

Key words: soot formation, polycyclic aromatic hydrocarbons, fullerenes, combustion, nanocarbon tubes.

INTRODUCTION

Soot formation is an important and constantly studied aspect of combustion, which has practical significance in the production of technical carbon as an active filler in rubber products and as a component of printing paints, as well as in energetic problems of hydrocarbon power plants and ecological issues [1–3].

Investigation of soot formation and oxidation is of special importance for several reasons. On the one hand, soot is a commercial product, whose world production is estimated at 10^7 tons per year. Black soot (technical carbon) is used as a filler for elastomers (90% of technical carbon is utilized for this purpose, 2/3 of them in tyre production) and in copy machines and laser printers. On the other hand, soot is known to be one of the main environmental pollutants. For example, direct-injection diesel engines first convert ≈10–20% of the fuel to soot. To understand the complex soot formation processes, one needs adequate models that should be tested by measuring particle concentration, particle size distribution, volume fraction of soot, etc. [3]. It is important that the indicated parameters be measured *in situ* by nondisturbing methods. Optical techniques, especially laser diagnostic methods are the most suitable for the indicated purposes. In addition to being nondisturbing, they have high spatial and temporal resolutions, which is especially useful in studies of soot formation and oxidation in turbulent flames.

[1] Al-Farabi Kazakh National State University, Almaty 480078; anara@kazsu.kz.

At present, a wealth of experimental material on soot formation has been accumulated and various phenomenological models have been proposed [1–11]. However, the soot formation mechanism is still not completely understood. In even seemingly simple cases, for example, homogeneous hydrocarbon pyrolysis, there is no full understanding of the process because it involves many fast parallel reactions resulting in a new solid phase — soot particles (for example, the time of conversion of methane with a molecular weight of 16 amu to soot particles with a molecular weight of 10^6 amu is 10^{-4}–10^{-2} sec).

Soot formation have been studied under various conditions: flames (premixed and diffusion), high-temperature reactors, and shock tubes.

1. PHENOMENOLOGY OF SOOT FORMATION

According to the laws of thermodynamics, in a premixed fuel–air system at standard flame temperature, solid carbon should appear at a mixture ratio (ratio of carbon to oxygen atoms) $C/O \approx 1$ [5], which is not always the case. Soot formation begins, except in detonations, at C/O ratios that are less than 1 and depend on the type of fuel. Some typical threshold parameters of soot formation $(C/O)_{cr}$ for almost adiabatically burning flames are presented in Table 1 [5, 8]. We note that in most of the Bunsen burner flames, except in C_2H_2–air, soot is released at the cone tip. The different values of $(C/O)_{cr}$ in burners of two types (Table 1) are due to differences in temperature and in the process of formation of polycellular flame.

TABLE 1

Soot Formation Threshold $(C/O)_{cr}$ for Premixed Flames ($p = 1$ bar, $t = 293$ K) [5, 8]

Mixture	$(C/O)_{cr}$	
	Bunsen burner	Flat flame
C_2H_6–air	0.48	0.47
C_3H_8–air	0.47	0.53*
C_3H_8–O_2	—	0.67*
C_2H_4–air	0.6	0.62
C_2H_4–O_2	—	0.7
C_4H_8–air	0.48	—
C_6H_6–air	0.57	0.62*
Methylnaphthalene–air	0.42	—
C_2H_2–air	—	0.83

Note. The values for multicellular flames are marked by an asterisk.

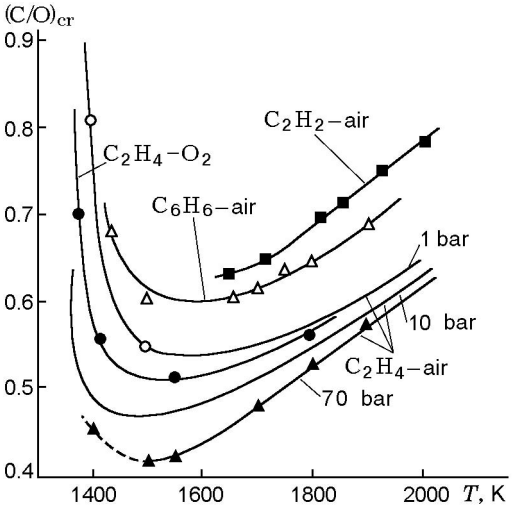

Fig. 1. Soot threshold $(C/O)_{cr}$ versus flame temperature for C_2H_4–air mixtures at various pressures and for C_2H_4–O_2, C_2H_2–air, and C_6H_6–air mixtures at $p = 1$ bar [12].

The results presented in Table 1 show that soot formation is controlled by the kinetics and occurs in flames under oxidation conditions. In postflame gases with C/O ratios somewhat lower than the soot formation threshold there are the same unburned hydrocarbons present as in mixtures with ratios $C/O > (C/O)_{cr}$. Therefore, the main processes of soot formation in the flames occur in the main reaction zone, in which there is competition between the oxidation and formation of sufficient concentrations of higher hydrocarbons.

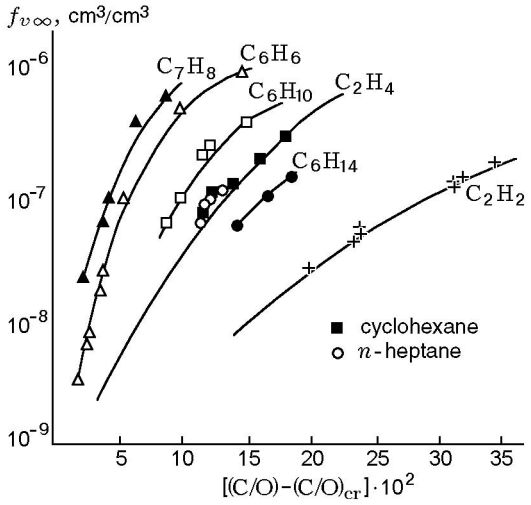

Fig. 2. Final volume fraction of soot versus excess of carbon for fuel–air flames from flat burners at normal pressure [12].

The soot formation thresholds depend on temperature and pressure, as is illustrated in Fig. 1 [12]. The curve shape in this figure, which is identical for the different mixtures and pressure, shows that there is not one but two thresholds for the C/O ratio at two different temperatures. With a pressure rise, the minimum of the $(C/O)_{cr}$ ratio is shifted toward the stoichiometric mixture ($C/O = 0.33$ for C_2H_4–air mixtures).

In the lower-temperature region, the values of $(C/O)_{cr}$ increase as the temperature decreases. Below 1 350–1 400 K, the burned gas contains a substance with a high molecular weight, but at such a low temperature, it cannot be transformed to soot for a time of contact $t < 0.1$ sec. For the indicated substance, the H/C ratio is approximately unity but its components are not identified. It should be noted that this low threshold temperature is similar to that observed on the center line of laminar diffusion flames at the beginning of soot formation.

In passing from the soot formation threshold in Fig. 1, where the mass concentration of soot is about 10^{-9} g/cm^3, toward high values of C/O, one observes a strong increase in the fraction of the final volume of soot $f_{v\infty}$ with respect to the volume of the flame gas. The curves in Fig. 2 qualitatively show how effectively the excess of carbon over the corresponding soot formation thresholds is converted to soot for various fuels [12].

Information on the conversion of burning hydrocarbon fuels to polycyclic aromatic hydrocarbons (PAHs) and soot [11] is shown diagrammatically in Fig. 3. PAHs are usually formed under conditions of rich mixtures and can have carcinogenic properties (as, for exam-

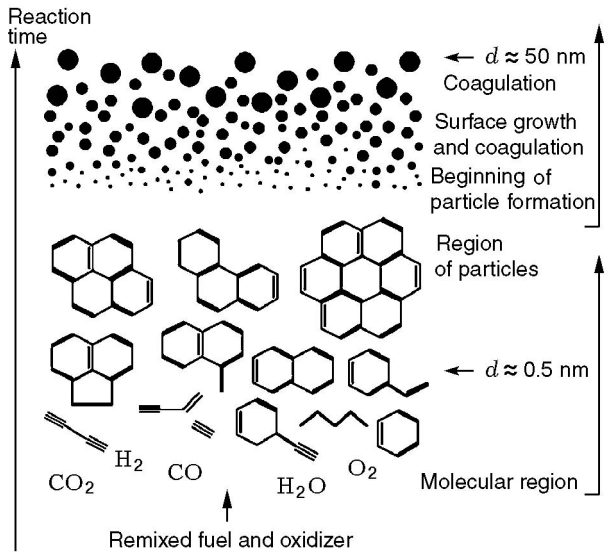

Fig. 3. Schematic diagram of soot formation in homogeneous systems or in premixed flames [11].

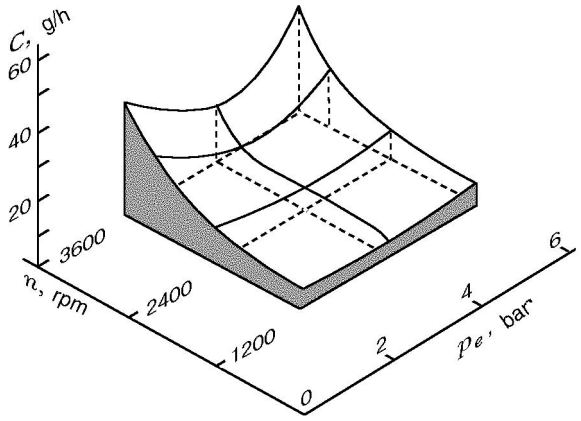

Fig. 4. Soot emission parameters for a four-cylinder diesel engine of volume 2.4 liters [5].

ple, benzpyrene). It is generally agreed that PAHs are important precursors (nuclei) of soot particles with a molecular weight of 500–2000 amu. The further particle growth is due to the surface growth in reactions involving many acetylene molecules and coagulation. Oxidation of soot particles occurs primarily in nonpremixed mixtures after the addition of oxygen-containing gases.

2. SOOT FORMATION IN DIESEL ENGINES

Soot particles are formed in the region between the fuel-rich side of the reaction zone of the diffusion flame and the fuel spray. The soot formation process can be regarded as a transition from the gas phase to a solid phase [5] with an extremely complex nature of conversion of the hydrocarbon fuel molecules containing a few carbon atoms to carbonaceous particles containing a few millions of carbon atoms. The finest particles are first formed by coagulation of PAHs. After that, the soot concentration increases as a result of adsorption of PAHs and especially as a result of particle surface reactions that increase this surface. This process involves hydrogen detachment and carbon attachment [13]. The primary particles coagulate into large aggregates, which are not necessarily found in the diesel exhaust gases. Their detection strongly depends on the temperature and time of conversion of the particles in the oxidizing medium. Therefore, only a few thousandth of the initially formed mass of soot is not completely oxidized and enter the diesel exhaust gases.

The soot emission from diesel engines constitutes a considerable part of the atmospheric aerosol even under proper operating conditions and depends on the engine performance. In some regions of Germany, the soot content in aerosols reaches 20%. The soot emission from a four-cylinder diesel engine of volume 2.4 liters [5] is shown in Fig. 4. It is evident that at 2500 rpm, the emission is relatively low but increases as the velocity becomes higher.

Soot emission from diesel engines is influenced by the atomization and configuration of the spray, the method of air supply, turbulence level, pressure, injection time, and ignition delay [14].

Studies of engine exhaust soot have shown that the particle size distribution depends weakly on the operating conditions and type of engine. The mean particle diameter is about 200–300 Å. In soot samples from exhaust systems or those collected at low exhaust temperatures there are heavy hydrocarbons condensed into agglomerates and converted to tarry material; in this case, the H/C ratio increases to unity.

The injection time, as mentioned above, is a very important factor. Early injection [15] allows one to inject more fuel, evaporate it, and mix it with air before ignition. High injection rates can also reduce soot formation. Increasing the air supply temperature reduces the ignition delay and, hence, promotes soot formation [14]. As noted in [1], the real values of the C/O ratio should, whenever possible, be kept close to the critical values since the volume fraction and particle size of soot increase as the C/O ratio grows.

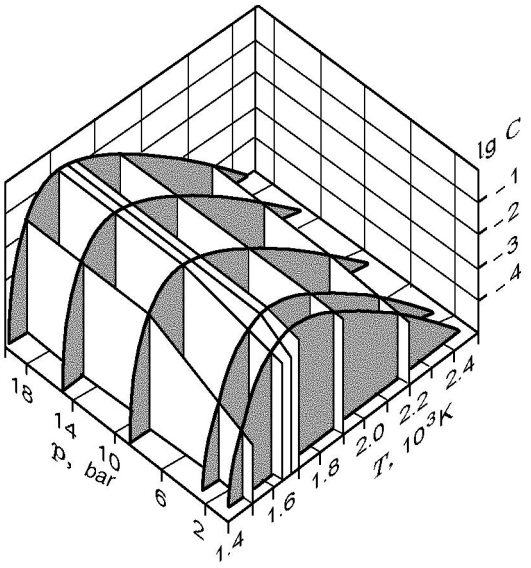

Fig. 5. Amount of soot (fraction of C atoms in soot particles) versus pressure and temperature [17].

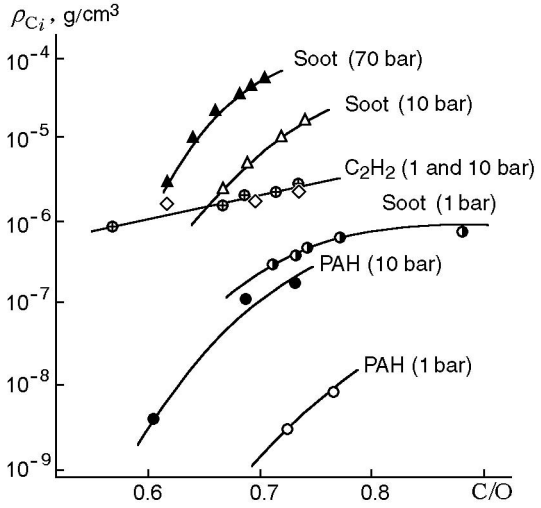

Fig. 6. Carbon density versus the C/O ratio for acetylenes, PAHs, and soot at various pressures [18].

3. PRESSURE EFFECT ON SOOT FORMATION

The pressure effect on soot formation can be interpreted as the effect of increased density of carbon atoms at elevated pressure. This assertion was verified in experiments on combustion of ethylene mixtures with oxygen and other oxidizers ($p = 1$ bar) [15]. In these experiments, the reaction zone was spatially resolved. The density of carbon atoms in soot particles was three times higher than their density in the corresponding air flames. The coagulation coefficients in these flames were constant.

Observations of coagulation in flames with high densities of carbon atoms under normal pressure agree with the findings of [8, 15, 16] obtained for C_2H_4–air flames burning at high pressures, and support the assertion on the effect of elevated density of carbon atoms.

The volume fraction of soot increases with a rise in pressure and the C/O ratio, and the temperature dependence is described by a bell-shaped curve [17] (Fig. 5). The latter is due to two circumstances. Soot formation requires precursor radicals; therefore, this process does not go at low temperatures. In addition, soot precursors undergo pyrolysis and oxidation at elevated temperatures, so that the soot formation process is limited by the range of $T = 1000$–2000 K.

Curves of carbon density versus C/O ratio for soot, PAHs, and C_2H_2 at $p = 1$, 10, and 70 bar [18] are given in Fig. 6. It is evident that pressure increases the rate of formation of PAHs and soot. The C/O ratio also influences the volume fraction of soot: an increase in the latter with increasing C/O ratio is also possible at high pressures.

Above the particle formation threshold, the density of soot carbon increases. For large values of C/O, the increase in the carbon density slows down. The dependence ρ_C (C/O) is stronger at $p = 10$ and 70 bar than at $p = 1$ bar. From Fig. 6, it is evident that an increasing amount of carbon fuel is converted to soot as the pressure rises.

In PAHs, the carbon density is two orders of magnitude lower than that in soot but the dependences of the carbon density of soot and PAHs on the C/O ratio at various pressure are very similar. From the data obtained, the following expression can be written:

$$\rho_C(\text{soot, PAH}) \approx [(\text{C/O}) - (\text{C/O})_{cr}]^{2.5-3}$$
$$\text{at } T > 1700 \text{ K and } 1 \leqslant p \leqslant 10 \text{ bar.}$$

At pressures above 10 bar, most of the carbon is converted to CO and CO_2.

The most striking finding is the strong decrease in the C_2H_2 concentration at $p > 10$ bar. At $p = 70$ bar, its concentration is below the detection limit.

4. FULLERENES AND THEIR FORMATION DURING COMBUSTION

As is known, in nature there are two allotropic forms of carbon — transparent solid diamond and layered soft graphite. In 1968, Sladkov with associated from the Institute of Petrochemical Processing of the

USSR Academy of Sciences synthesized a third allotropic form of carbon — carbine, a white substance with a density intermediate between the densities of diamond and graphite.

C_{60} and C_{70} fullerenes were identified in 1985 [19] and obtained in macroscopic quantities in 1990 by graphite vaporization in an arc discharge. In 1988 and 1991, C_{60} and C_{70} fullerene ions were extracted in significant amounts from flame and identified spectroscopically [20, 21]. Howard [22] found considerable amounts of C_{60} and C_{70} in low-pressure premixed laminar benzene–oxygen flames. The greatest concentration of $C_{60} + C_{70}$ was 20% of the resulting soot. The maximum rate of formation of $C_{60} + C_{70}$ was observed for $p = 69$ torr, C/O = 0.989, and dilution with 25% helium. In the fullerenes produced in flames, the C_{70}/C_{60} ratio was in the range of 0.26–8.8, whereas for graphite vaporization, $C_{70}/C_{60} = 0.02$–0.18.

Fullerenes are a class of exclusively carbon compounds with polyhedral closed-shell structure. They were identified as ionized particles in low-pressure fuel-rich flat premixed acetylene and benzene–oxygen flames by molecular-beam sampling combined with mass-spectrometer analysis [20].

Later, macroscopic quantities of various fullerenes, not only such as C_{60} and C_{70} [21, 23] but also larger species up to C_{116}, were extracted by solvents from the soot formed in low-pressure premixed laminar benzene flames [24].

The yield of C_{60} and C_{70} was 20% of the weight of soot and 0.5% of the weight of the starting fuel carbon [25]. The relationship between fullerenes and soot formation was theoretically established by Zhang et al. [26] after the discovery of fullerenes in experiments with laser vaporization of graphite [19]. The reactions of fullerene and soot formation in an arc discharge have much in common with the reactions in rich fuel flames. Bulbous fullerene nanostructures were detected along with fullerenes in soot using high-resolution transmission electron microscopy [27].

Figure 7 gives concentration profiles of fullerenes and soot and the temperature profile in a benzene–oxygen–argon flame (C/O = 0.88) [23]. It is evident that fullerenes are formed after the main stage of soot formation. As the C/O ratio increases from 0.88 to 0.96, the fullerene concentration increases monotonically.

Grieco et al. found [28] that in the flame reaction zone, the quantity of closed-shell structures in soot, as well as the fullerene concentration in the gas phase, increases with increasing residence time. At a distance of more than 70 mm above the burner, the fullerene concentration decreased, and at a distance between 60 and 120 mm the concentration of closed-shell structures

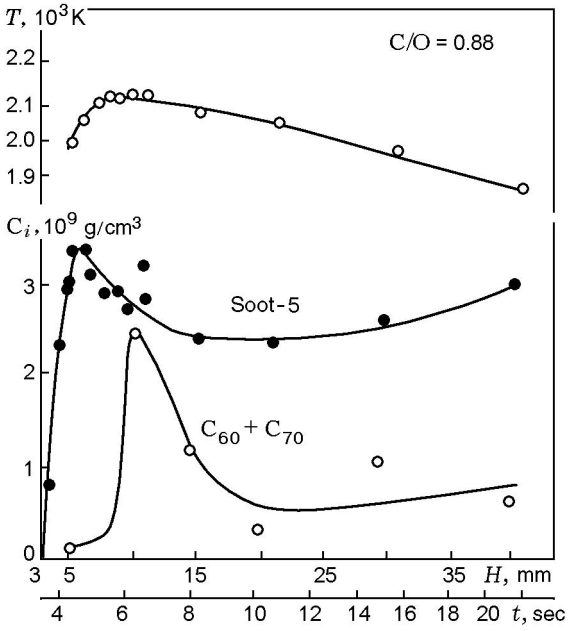

Fig. 7. Concentration profiles of fullerenes and soot and the temperature profile in a benzene–oxygen–argon flame [23](H is the distance from the burner).

decreased. The transition from amorphous to fullerene carbon can be explained by deposition gas-phase particles, such as PAHs, on soot particles. The particle deposition is accompanied by internal redistribution of solid-state carbon and by reaction between gas-phase fullerenes and the growing soot particles, which is consistent with the consumption of fullerenes at a distance beyond 70 mm above the burner. Highly ordered nanostructures such as nanotubes and fullerene bulbs were detected in solid samples collected from the walls and top of the combustion chamber, indicating that they formed during the internal redistribution processes occurring in solid-state carbon for a time not exceeding 100 msec. This conclusion is consistent with the formation of closed-shell species by intense thermal treatment of the initially disordered, insoluble part of the fullerene-containing soot generated in an electric arc discharge [29].

In contrast to the proposed role of fullerene structures as soot precursors [26], the results of [30] indicate parallel growth of gas-phase fullerene molecules along the vertical in flame. In addition, it is found [31] that the nucleation of soot particles is accompanied by deposition of fullerenes on them.

Frenklach and Ebert [25] explain fullerene formation by successive buildup of bent structures, i.e., PAHs containing five- and six-membered rings. They believe that in flames bent PAHs should be less abundant

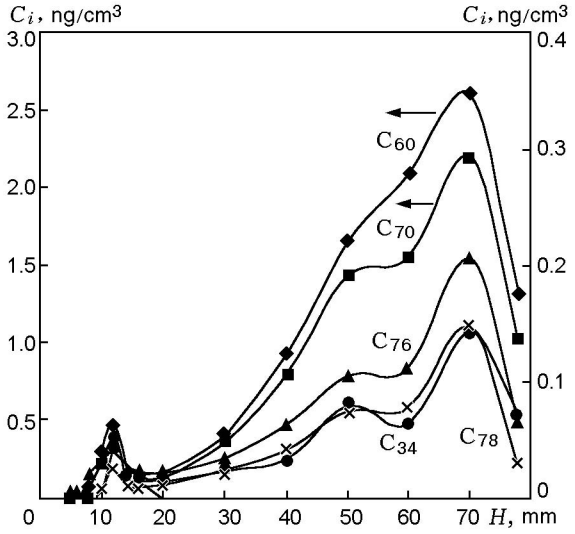

Fig. 8. Fullerene concentrations profiles on the axis of a premixed benzene–oxygen–argon flame [28].

than planar PAHs, which is supported by measurements of concentrations of PAHs (including corannulene — a bent molecule) in fullerene-forming flames [32].

Corannulene is a subsystem of almost all fullerenes and is therefore of special interest as a precursor of fullerenes. Corannulene occurs in detectable concentrations in ethylene–air flames at atmospheric pressure, in which fullerenes have not been detected, but in large concentrations it was found in low-pressure fullerene-forming benzene flames [33].

The kinetic validity of the mechanism of fullerene formation by successive gas-phase reactions is shown by Baum et al. [34]. Based on calculations for a plug-flow reactor with experimental concentrations of various species as input data, the authors described the formation of C_{60} and C_{70} fullerenes beginning with fluoranthene and the subsequent growth by successive steps of hydrogen detachment and the addition of C_2H_2 with corannulene as an intermediate compound.

The formation of C_{60} and C_{70} fullerenes by detachment of hydrogen and the addition of C_2H_2 was also tested by modeling a low-pressure fullerene-forming flat premixed benzene-oxygen–argon flame at an equivalence ratio of 2.4 [34].

The concentrations profiles of fullerenes [28] are characterized (Fig. 8) by two local maxima, the first of which is smaller. Studying the evolution of the concentrations of fullerenes, PAHs, and soot with increasing distance above the burner, Grieco et al. [28] draw the conclusion that the first maximum may be due to the reactive coagulation of PAHs, accompanied by intramolecular condensation, including dehydrogenation, rearrangement, and ring formation.

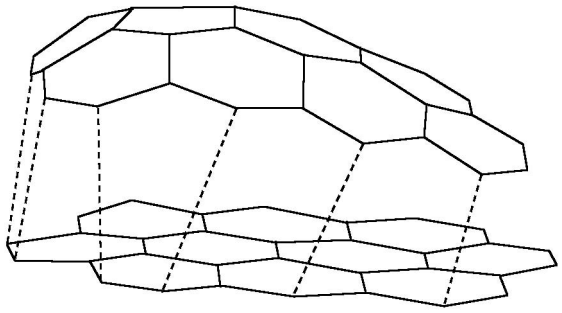

Fig. 9. Model for the formation of five- and six-membered rings through the linkage of two PAHs by the zipper mechanism [37].

Apparently, PAHs are mostly consumed in soot formation, and to a lesser extent in fullerene formation. Grieco et al. [28] concluded that the second concentration maximum, which is in the region of the most intense fullerene formation, cannot be attributed to reactions involving PAHs alone, whose concentrations in this region are at or below the detection limit of analytical equipment, but it can be explained by sequential attachment of acetylene to PAHs.

The pathways of fullerene formation in flames have been extensively studied by Homann's group using direct input of ionic and neutral species into a mass spectrometer [30, 35, 36]. Experiments combining molecular-beam sampling with mass-spectral analysis were performed with low-pressure premixed flames of acetylene [37], benzene [38], butadiene and naphthalene [37] with oxygen. The important role of bimolecular reactions between two PAHs involving coordinated detachment of hydrogen (the so-called zipper mechanism) in the growth of fullerenes was explained [37]. The reaction starts with a sandwich-type arrangement of two recondensed PAHs (Fig. 9) and has a distinctive feature such as the formation of exactly 12 pentagons, which are larger or equal to coronene ($C_{24}H_{12}$), irrespective of the size of the PAHs. At the same time, by the zipper mechanism, the pentagons should be brought to the thermodynamically most favorable positions, for example, by pyracylene rearrangement [39, 40]. Some experimental evidence of the zipper mechanism has been obtained. Thus, hydrogenated species such as $C_{60}H_x$ ($1 < x < 6$) [37] were predicted, and the shape and location of their concentration profiles agree with those of the precursors of the corresponding fullerenes. Furthermore, a new class of carbon molecules — the so-called aromers, which are negatively charged ions produced by the reaction of two PAHs — was proposed. Aromers are represented as hydrogen-rich PAHs — species with a rather low level of structural packing, direct precursors of fullerenes [38].

The formation of fullerenes requires a number of single-step monomolecular reactions, such as cage closure, C—H bond rupture, and intramolecular rearrangements, and, therefore, a high temperature of the process is preferred. In conclusion, a combined mechanism for fullerene formation can be presented. Taking into account the geometrical incompatibility of the majority of aromers for the growth of fullerenes as the final products of the reaction between different PAHs, it is assumed that the reactions with acetylene can lead to a further growth of the molecules up to the geometrical compatibility for required for cage closure.

Finally, the flames suitable for the synthesis of macroscopic quantities of fullerenes [23, 24] are characterized by higher values of C/O than the flames from which molecular-beam sampling can be performed [30, 38]. The processes of soot and fullerene formation along the flame axis at high C/O ratios, where substantial quantities of fullerenes are produced, are apparently similar, and, hence, the contribution of the condensed-phase formation pathways cannot be ruled out.

5. FORMATION OF NANOCARBON TUBES AND NANOFIBERS IN FLAMES

Recently, there have been a number of papers on the synthesis of carbon nanotubes using flames as a heat source. The production of carbon nanomaterials (such as nanotubes and nanofibers) in flames has a number of advantages over the production processes using electricity. First, flame as a heat source is far less expensive than electricity. Second, the synthesis in flames are more suitable for measurements than the methods based on electricity [41]. Yuan et al. [42, 43] found multiwalled carbon nanotubes on a nickel–chromium wire and on a stainless steel mesh in diffusion flames.

For C_2H_2 diffusion flames, Vander Wal et al. [44] studied the relative contribution of the electronic structure and chemical composition using Cu, Fe, and Ni, as catalysts and Al_2O_3, CaO, SiO_2, and TiO_2 as supports. Those studies showed that the electronic interaction between the metal catalyst and the support considerably influences the density, the homogeneity, and structure of the carbon nanotubes. In [45, 46], a fuel-rich premixed flame served as a heat source and a thin wire mesh of stainless steels (grade 304) coated with cobalt was used as the catalyst. The postflame gas mixture was studied in equal proportions with various fuels to determine the optimal conditions for the growth of nanotubes in using hydrocarbons. The authors [45, 46] came to the conclusion the optimal molar fractions of CO and H_2 equal $\approx$0.105, which can be implemented using an ethylene–air mixture in a proportion of 1.62.

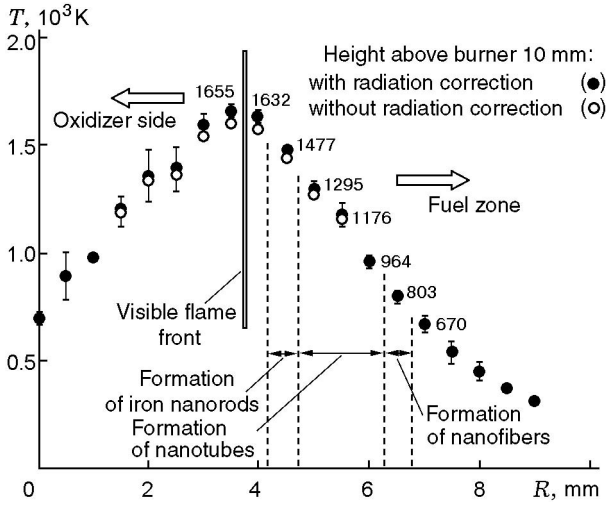

Fig. 10. Radial temperature distribution showing three zones of formation of nanomaterials [51].

Saveliev et al. reported [47] on the synthesis of carbon nanotubes in oxygen-rich opposed-flow methane flames. Straightened "bean-sprout-like" nanotube bundles were synthesized in a methane diffusion flame by Yuan et al. [48]. In the experiments of Merchan-Merchan et al. [49], a thick layer of vertically aligned carbon nanotubes on the surface of a catalytic sample was detected using an opposed-flow flame with controlled electric field.

The typical temperature for the synthesis of carbon nanotubes and nanofibers in diffusion flames with catalytic methane is lower than the soot-formation temperature. The findings of [42, 43] suggest that the formation of carbon nanotubes and nanofibers on a catalytic support occurs inside the soot-formation zone of a normal diffusion flame. Unlike in diffusion flame, however, the formation of carbon nanotubes and nanofibers on a catalytic support can occur outside the soot-formation zone, which is also located outside the flame front.

Carbon atoms as a source of graphite layers, catalytic metals for the conversion of gas-phase carbon atoms to solid graphite layers, and heat sources for the activation of the catalytic metals are three important factors in the synthesis of carbon nanomaterials in flames. Lee et al. [50] studied the synthesis of carbon nanotubes and nanofibers on a metal support coated with $Ni(NO_3)_2$ in an ethylene inverse diffusion flame as a heat source.

Figure 10 shows the gas temperature distribution at the flame front [51], illustrating three zones of formation of nanomaterials using a support coated with $Ni(NO_3)_2$. The maximum gas temperature was 1655 K at 3.5 mm from the flame axis. In the temperature range of 1400–900 K, carbon nanotubes of diameter 20–60 mm

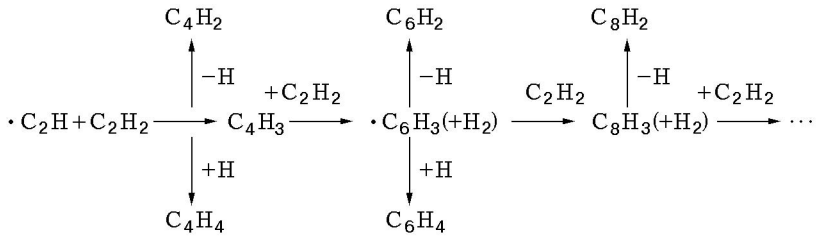

Scheme No. 1.

formed. At $T > 1400$ K and $T < 900$ K, iron nanorods and carbon nanofibers, respectively, were synthesized.

6. FORMATION OF CARBON MACROPARTICLES DURING PYROLYSIS OF HYDROCARBONS

Carbon (soot) macroparticles are associated primarily with exhaust gas emissions from a powerful diesel engine or pyrolytic equipment. Diesel engine soot is an undesirable product that reduces the service life of engines, pollutes the environment, and is a hazard to man's health since soot particles contain molecules of polyaromatic hydrocarbons. For example, for trucks of moderate power, the U.S. regulation limits the exhaust of particles to 0.05 g/(kW · h) [52]. Soot, however, is also produced commercially with strictly monitored operating conditions and is used in the production of trunks and gums. This kind of soot is called technical carbon.

Studies of soot formation during pyrolysis of pure hydrocarbons and hydrocarbon mixtures under isothermal conditions have shown that: 1) sooty aerosols with high activation energies are formed [53–56]; 2) there are quantitative relations for the soot formation tendency of hydrocarbon [54–56]; 3) the inhibition of soot particle nucleation is observed during pyrolysis of hydrocarbon mixtures [53, 56–58].

The temperature and concentration of the hydrocarbon subjected to pyrolysis and the gas residence time in the pyrolytic system are the main factors determining the soot formation of carbon macroparticles.

In the experiments of Shurupov [58], benzene, acetylene, carbon tetrachloride, and methane diluted with helium were pyrolized in a jet-flow reactor under nearly isothermal conditions (at $T = 1373$–1673 K) with a gas residence time of up to 125 msec. The effects of the temperature and initial concentration of the hydrocarbons on the beginning of formation of disperse carbon and the number density of soot particles were studied. Empirical equations were obtained that describe the induction period of soot formation τ_{ind} for the isothermal pyrolysis of benzene, acetylene, carbon tetrachloride, and methane with variations in the concentration of the substance subjected to pyrolysis and temperature:

$$\tau_{\text{ind}} = (6.3 \pm 0.8) \cdot 10^{-12} [\text{C}_6\text{H}_6]^{-0.8} \exp(26{,}700/T),$$

$$\tau_{\text{ind}} = (3.2 \pm 0.5) \cdot 10^{-9} [\text{C}_2\text{H}_2]^{-0.9} \exp(19{,}000/T),$$

$$\tau_{\text{ind}} = (4.3 \pm 0.7) \cdot 10^{-9} [\text{CCl}_4]^{-0.9} \exp(18{,}700/T),$$

$$\tau_{\text{ind}} = (9.0 \pm 1.5) \cdot 10^{-10} [\text{CH}_4]^{-0.9} \exp(21{,}600/T)$$

(τ_{ind} in seconds).

The differences in the induction period of soot nucleation for different hydrocarbons can be explained by the inhibition effect of soot particle formation. The experiments showed that during pyrolysis of hydrocarbons diluted with helium, the concentration of soot particles is constant for contact times of 10–125 msec.

7. SOOT FORMATION MECHANISM

Many researchers regard polycyclic aromatic hydrocarbons as precursors of soot particle nuclei. Thus, in an acetylene–oxygen diffusion flame, Homann and Wagner [8] found two types of polyaromatic molecules:

1) polycyclic aromatic compounds without side chains: naphthalene, acenaphthalene, coronene, and phenanthrene;

2) polycyclic aromatic compounds with side chains (a molecular weight of 150–500).

The concentration of polyaromatic compounds of the first group remained almost unchanged in the soot-formation zone, whereas the concentration of PAHs of the second group increased sharply.

In the zone of intense soot formation, one can distinguish one more large group of molecules — polyacetylenes, which are intermediate products from the formation of polyaromatic compounds. Homann and Wagner [59] proposed a model for the formation of polyacetylenes by scheme No. 1.

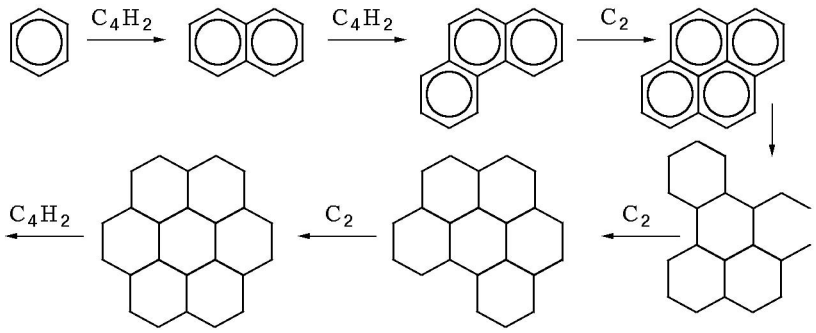

Scheme No. 2.

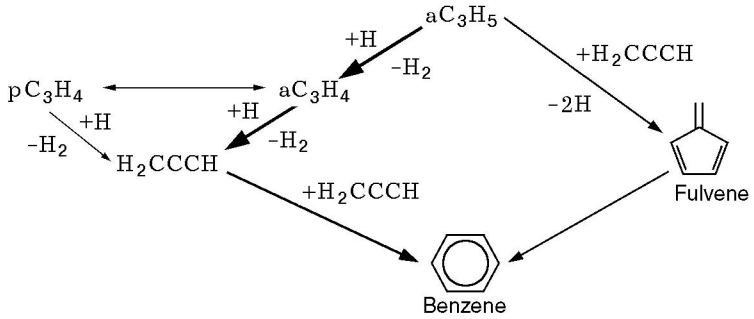

Fig. 11. Benzene formation pathways in a methane diffusion flame.

Using a thermochemical group method, Stein and Fank [60] estimated the transformation energetics for some PAHs and then calculated the equilibrium constants between PAHs and H_2 and C_2H_2. For the first six products of the thermodynamically most favorable pathway of PAH polymerization, transformation scheme No. 2 was proposed. Here the notation C_2 and C_4H_2 should be understood as symbols that denote the number and type of atoms attached in each polymerization step and not as chemical reactants. An important finding of this work was that at $T > 1700$ K, the homogeneous equilibrium system contains some "critical," strongly condensed PAHs, whose concentration is minimum over a wide range of ambient conditions. This implies that in the high-temperature homogeneous systems there is a thermodynamic barrier for soot formation.

By modeling, Miller and Melius [61] showed that there are two main pathways of benzene formation in fuel-rich premixed diffusion flames and both of them include resonance-stable radicals. These pathways are illustrated in Fig. 11. They include the reaction of allyl and propargyl radicals and the spontaneous reaction of propargyl radicals.

The formation of aromatic compounds and PAHs in industrial combustion was modeled using a detailed chemical kinetic model [62]. The highly turbulent, highly reactive zone of a typical industrial diffusion flame was represented using the model of a perfect-mixing reactor. This model was employed to determine the emission of aromatic compounds and PAHs with variation in the equivalence ratio. In the full-scale industrial furnace at the Sandia National Laboratories, the temperature in the perfect-mixing reactor presumably equalled to 1500 K. The fuel composition was chosen so as to be similar to that used in experiments: 16% H_2, 7.3% propane, and 76.7% natural gas. For an approximate determination of the benzene concentration in the exit gas, the deposition time was set equal to 10 sec. A comparison of the calculated and experimental results is given in Fig. 12. It is evident that the detailed chemical kinetic models may be useful for interpreting experimental data.

Experimental and calculated and theoretical simulation of soot formation during hydrocarbon oxidation in shock waves is dealt with in [65].

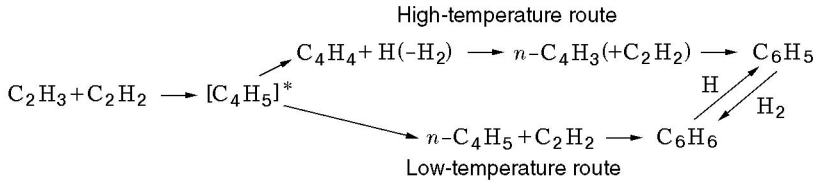

Scheme No. 3.

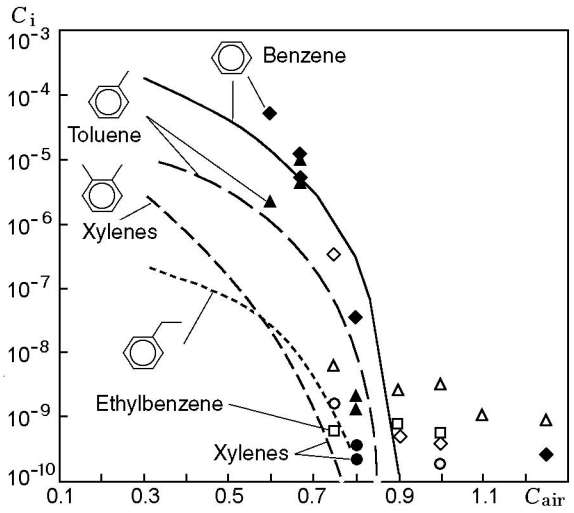

Fig. 12. Comparison of the experimental data of [63] (open points) with the results of detailed chemical kinetic simulations in [64] (filled points.

7.1. Formation of the First Aromatic Ring

In flames of nonaromatic fuels, the formation of the first aromatic ring starts with the joining of vinyl and acetylene. At high-temperatures, this ring is formed by a combination of acetylene with the n-C_4H_3 radical produced by detachment of H from vinyl acetlylene H. At low temperatures, the interaction of acetylene with vinyl yields n-C_4H_5, which leads to benzene formation. Benzene and phenyl radicals can be transformed by the same reaction of H detachment (see scheme No. 3).

Urmashev et al. [66] performed calculations in the temperature range of 1500–2500 K at a fuel/oxidizer ratio of 4 : 1, 3 : 1, 2 : 1, 1 : 1, and 1 : 2. They studied the radical chain mechanism of methane combustion that included 87 elementary reactions. The values of the preexponents, activation energy, and reaction orders were taken from [17]. For reaction Nos. 60–87, these constants are unknown and were varied so as to obtain the maximum concentration of PAHs. The preexponent was varied in the range of 10^{12}–10, which corresponds to the transition from the radical mechanism to the ionic mechanism of formation of polycyclic hydrocarbons.

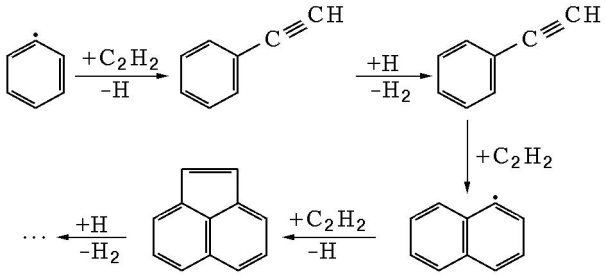

Scheme No. 4.

7.2. Soot Formation Mechanism in Flames

Krestinin et al. [67] developed a kinetic model of soot formation that treated the formation of primary sooty aerosol as the chemical condensation of "supersaturated polyene vapor."

During the induction period of soot formation, the hydrocarbon molecule of the starting substance is pyrolized, resulting in two main families of hydrocarbons: polycyclic aromatic and polyene molecules. As compared to the rather slow increase in the number of aromatic rings in the PAH molecule, which requires five to seven elementary stages, the growth in the length of the polyene molecule proceeds in one stage:

$$C_{2n}H_2 + C_2H = C_{2n+2}H_2 + H, \quad n = 1, 2, 3 \ldots .$$

As a result, the concentrations of C_4H_2, C_6H_2, C_8H_2, etc., polyene molecules reach high values, and polyenes are found among the main intermediate products of decomposition of the starting hydrocarbon in flames and in the pyrolysis processes. This fact, together with the extremely high reactivity of polyenes in polymerization reactions, became the main argument in favor of the assumption that exactly these molecules are gaseous soot precursors, which forms the basis of the polyene model.

The theoretical development of the aromatic path of soot formation consisted of showing how the aromatic components can coagulate to form primary aerosol particles. One of the pathways for the growth of PAHs and soot was the mechanism proposed in [70], which involves a sequential buildup of cycles in the reactions involving acetylene (the mechanism of hydrogen detach-

ment and attachment of C_2H_2; see scheme No. 4). The significance of this reaction was confirmed even in the first attempt to numerically model the growth kinetics of aromatics.

7.3. Detail Modeling of Formation of PAHs and Soot

It is believed that polycyclic aromatic hydrocarbons are the key intermediate compounds in soot formation [68–70]. Recently, there has been wide use of a scheme for the evolution of soot formation that consists of the following parallel processes.

(a) Particle nucleation. PAHs of large sizes are formed primarily by sequential chemical reactions of radicals of small-size PAHs with acetylene, PAHs, and PAH radicals. Having a definite size, different kinds of PAHs interact with each other, whereas individual PAHs continue to grow; particle formation (nucleation) occurs.

(b) Surface growth. The reactions on the surface of the growing particles considerably promote the accumulation of the carbon mass. It is assumed that such reactions are similar to the reactions of PAHs [68–70], whose reactant sides are activated by hydrogen detachment, while the growth competes to the oxidation involving O_2, OH, and O. Acetylene and PAHs are growth species; their relative contribution, apparently, depends on the conditions of the process [71–74]. The decrease in the surface growth rate due to an increase in the particle sizes agrees with decreases in the experimentally observed H/C ratios [75–78].

(c) Particle coagulation. Subsequently, the particle sizes increase upon the collision of the growing soot particles. Initially, the colliding particles completely coalesce with the formation of new spherical structures, and later they agglomerate into fractal clusters, i.e., chain-like structures [70].

Richter et al. [79] developed a detailed kinetic model that describes the formation and consumption of PAHs and soot during combustion of fuel-rich mixtures. The reaction mechanism consists of 1102 gas-phase reactions and 5502 reactions that describe the growth of soot particles with the participation of 295 species. Using a sectional approach, large PAHs and carbon particles of diameter 70 nm are assigned to classes (Bins) that cover a definite range of mass numbers. The number of carbon and hydrogen atoms corresponding to their mean weights assigned to each Bin is explained by a decrease in the H/C ratio with increasing particle size. The model was successfully tested on a rich premixed benzene–oxygen–argon flame ($\phi = 2.4$, 10% Ar, $\upsilon = 25$ cm/sec, and 5.33 kPa). Preliminary calculations for the model were compared with literature experimental data, including profiles of molar fractions of individual PAHs and soot concentration profiles. It was found that the reactions of PAH radicals with PAHs and between PAH radicals were the main pathway to soot nuclei. The surface growth supplies ≈75% of the final particle weight, and the reactions of acetylene with radical species — the main pathway of development of the surface growth reaction — lead to a decrease in the PAH concentration in the postflame zone. The coagulation of particles, including Bin particles and Bin radicals, promotes the formation of particles of increasingly larger size, whereas the oxidation by OH radicals plays a minor role in their decrease.

For a better quantitative understanding, the detailed reaction schemes describing the formation and concentration decrease of PAHs [80, 81] were extended to particle formation [82, 83]. Many mechanisms are based on a scheme that assumes that PAHs of definite sizes is the soot core. At the same time, fast polymerization of acetylene was suggested as a pathway that leads to an increase in the size of carbon structures [84]. Two major principles were applied: the method of moments [82] and a sectional approach [83, 85]. In a discrete sectional reactor, the unification of particles is described by introducing classes (Bins). A characteristic feature of the sectional approach is similarity in the description of gas-phase and colloidal-chemical systems, which are directly related and are both written in the general form $A + B = C + D$.

The number of particles of identical weight and the number of structural isomers increase rapidly with increasing molecular weight. Therefore, the classes (Bins) of very large PAHs and particles covering definite ranges of weights were determined. The mean molecular weight and the number of carbon atoms and hydrogen correspond to each Bin. The characteristics of the Bins are given in Table 2. The diameters σ were determined assuming spherical structures and concentrations of 1.8 g/cm^3 [86]. The transition from gaseous to solid particles was assumed to depend on temperature and pressure. Based on the definition of compounds containing up to 160 carbon atoms in extracts of flame-generating condensed material [87], Bin Nos. 5 or higher can be treated as particles whereas Bin Nos. 1 to 4 are conceptually known as "large PAHs." This description agrees with the definition of particles with a molecular weight of ≈2000 amu and a diameter ≈1.5 nm as particles originating from soot particles [71, 88] and with the definition of soot as unextracted particles in the case of gravimetric determination of their concentrations [89]. It was found that the decrease in the H/C ratio and the resulting increase in the curvature are due to the pres-

TABLE 2

Definition of Classes of Molecules (Bins) That Describe Large PAHs and Soot Particles

Bin	Weight, amu	C_xH_y	σ, nm	H/C
1	201–400	$C_{24}H_{12}$	0.85	0.500
2	401–800	$C_{48}H_{24}$	1.07	0.500
3	801–1600	$C_{96}H_{48}$	1.34	0.500
4	1601–3200	$C_{193}H_{84}$	1.69	0.435
5	3201–6400	$C_{388}H_{144}$	2.13	0.371
6	6401–12,800	$C_{778}H_{264}$	2.68	0.339
7	12,801–25,600	$C_{1560}H_{480}$	3.37	0.308
8	26,601–51,200	$C_{3124}H_{912}$	4.24	0.292
9	51,201–102,400	$C_{6256}H_{1728}$	5.35	0.276
10	102,401–204,800	$C_{12528}H_{3264}$	6.73	0.261
11	204,801–409,600	$C_{25088}H_{6144}$	8.48	0.245
12	409,601–819,200	$C_{50240}H_{11520}$	10.69	0.229
13	819,201–1,638,400	$C_{100608}H_{21504}$	13.46	0.214
14	1,638,401–3,276,800	$C_{201472}H_{39936}$	16.96	0.198
15	3,276,801–6,553,600	$C_{403456}H_{73728}$	21.36	0.183
16	6,553,601–13,107,200	$C_{807936}H_{135168}$	26.91	0.167
17	13,107,201–26,214,400	$C_{1617920}H_{245760}$	33.91	0.152
18	26,241,401–52,428,800	$C_{3239936}H_{442368}$	42.72	0.137
19	52,428,801–104,857,600	$C_{6483968}H_{835584}$	53.83	0.129
20	104,857,601–209,715,200	$C_{12972032}H_{1622016}$	67.82	0.125

TABLE 3

Concentration of Propane Oxidation Products Versus the Temperature of the Second Reactor Section ($p = 40$ kPa, $T_1 = 300$ K, and $t = 10$ sec)

T, K	Partial pressure, kPa									
	C_3H_8	C_3H_6O	C_2H_4	C_2H_4O	CH_3O	CH_3CHO	CO	CO_2	CH_2O	Soot
663	1.02	0.08	0.1	—	0.05	0.04	0.2	—	0.04	—
684	0.97	0.05	0.08	—	—	—	0.16	—	—	—
696	1.28	0.11	0.16	—	—	—	0.38	—	—	—
723	2.25	0.36	0.61	0.05	0.1	0.06	1.22	0.05	0.09	+
740	2.97	0.57	1.22	0.11	0.19	0.09	2.03	0.08	0.16	+
768	2.61	0.4	2.6	0.2	0.3	0.2	2.93	0.15	0.25	+

ence of five-membered ring-type structural units and in many cases correlate with the formation of fullerene structures [31, 90]. In [79], the maximum particle diameter measured in experiments with a low-pressure one-dimensional homogeneous mixture in an acetylene flame [91, 92] was correlated with the value of H/C determined under similar conditions [59].

8. SOOT FORMATION IN COOL HYDROCARBON FLAMES AND THE FLAME FRONT STRUCTURE

The region of cool flames, as is known [93], covers the temperature range of 500–800 K for long-chain hydrocarbons to 800–1200 K for methane. Soot formation is often observed at the upper temperature boundary of cool flames, but because of difficulties in studying such flames, it is possible to exit from the soot formation regime by changing experimental conditions. At the same time, soot formation has never been treated as a transient phenomenon between cool and hot flames and low-temperature soot formation has not been studied in detail.

Pogosyan, et al. [94], studying the oxidation of propane–oxygen mixtures in a ratio of 1 : 1 in cool flames in the range $T = 720$–800 K, observed an oscillatory oxidation regime that was accompanied by soot formation. An analysis of the composition of the oxidation products (Table 3) suggests that there is a certain relationship between soot formation and increases in the concentrations of ethylene and carbon oxide and that the transformation mechanism may change upon a slight increase in the reactor temperature.

Bohm et al. [95], studying the influence of pressure and temperature on soot formation in flames of homogeneous mixtures of ethylene and benzene with air coined the term "cool sooting flames." It was shown that along with the high-temperature threshold there is a low-temperature threshold of soot formation. It is noted [95] that the properties of cool sooty flames differ from the properties of hot flames and have features in common with the pyrolysis of aromatic compounds. It is emphasized that a detailed analysis of the soot particles produced in cool flames is required to understand the nature and mechanism of low-temperature soot formation.

8.1. Experimental Technique and Analysis Methods

A description of the reactor, experimental technique, and results of identification of polycyclic aromatic hydrocarbons for low-temperature soot formation in rich flames of butane and propane corresponding to the upper temperature boundary cool flames are given in [96]. Soot formation in methane–oxygen rich flame was studied using the technique of flame stabilization in a separately heated, two-section reactor [96, 97]. The experiments were performed at atmospheric pressure and with temperature variation from 723 to 873 K in the first section and from 973 to 223 K in the second section. The contact time was 2.5–10.2 sec, and the $CH_4 : O_2$ component ratio was varied from 1.5 : 1 to 2 : 1.

During low-temperature soot formation in a burning a propane–oxygen mixture, a threshold maximum flame temperature was observed which was independent of the temperature of the second reactor section, probably indicating the existence of the limiting stage.

TABLE 4

Results of Powder X-Ray Analysis of Soot Samples [98]

T_2, K	t, sec	L_a, Å	L_c, Å	d_{002}, Å	n	Type of sample
973	7	54	15.5	3.64	4	Soot
1103	7	50.7	22	3.62	6	
973	7	42.7	24.3	3.55	7	Pyro-carbon

Note. 2/1 CH_4/O_2; $T_1 = 723$ K.

8.2. Radiography of Soot Particles

An analysis of the diffraction spectra (a DRON-1.5 diffractometer with a modified collimation, CuK_α radiation) of all examined soots [98] shows that they are a superposition of three X-ray amorphous phases: an oxygen-containing O-phase with peaks (002) at $\Theta_1 = 3.7°$, a boghead (or hydrocarbon) B-phase at $\Theta_2 = 9.4$–$10.0°$, and a crystalline prographitic G-phase at $\Theta_3 = 12.0°$. A comparative analysis shows that the diffraction spectra of the examined soots differ considerably from those of commercial samples of technical carbon, primarily by the presence of the O- and B-phases in them. On the other hand, the composition and quantitative ratio of the X-ray phases was close to natural coal formations — anthracites. Quantitative analysis showed that all examined soots have similar compositions with the content of the O-phase varying from 12 to 14% the B-phase from 27 to 31%, and the G-phase from 57 to 60%. The phases exhibited a diffraction coefficient $M = 63$–75%.

TABLE 5

Results of Soot Extraction for Low-Temperature Combustion of Methane and Propane [99, 100]

Sample number	Consumption of O_2, cm^3/min	T_1, K	T_2, K	Weight of dry residue	Yield of dry extract, %
Methane					
1	1150	832	873	223.1	22.31
2	1150	832	973	214.0	21.40
3	1150	832	1023	177.4	17.74
4	1400	298	298	301.5	30.15
Propane					
5	2450	423	773	502.5	50.25
6	2450	423	873	410.2	41.02
7	2450	423	973	220.0	22.00

Note. The weight of extracted soot is 1 g, the consumption of CH_4 is 2000 cm^3/min, and the consumption of C_3H_8 is 1600 cm^3/min.

The results of X-ray analysis of soot samples are given in Table 4 [98]. In the coherent-diffraction region, the parameters L_a, L_c, and d_{002} describing the structure of the soot packet constituting the particles of the sample are calculated from X-ray patterns. Here T_1 and T_2 are the temperatures in the first and second sections of the reactor, respectively, L_a is the cross-sectional size of the soot packet, L_c is its height, d_{002} is the distance between two adjacent layers in the soot packet, and n is the number of planar meshes.

8.3. Formation of PAHs in Low-Temperature Sooty Flames

Table 5 gives data on extraction of soots formed in methane and propane flame [99, 100]. The greatest amount of PAHs is 22.31% in methane soot and 50.25% in propane soot; in this case, the reactor temperature corresponding to the maximum content of PAHs decreased by 100 K with a considerable decrease in T_1. These data suggest that in the low-temperature combustion of methane and propane, PAHs are soot precursors.

During the extraction of the soots (technical carbon), it was found that 20–30% of the material passes to the extract. The data of chromatographic group analysis show that the extract contains up to 70% polyaromatic compounds, up to 17% resins, 10–11% asphaltenes, and 1–2% paraffinic and naphthenic hydrocarbons.

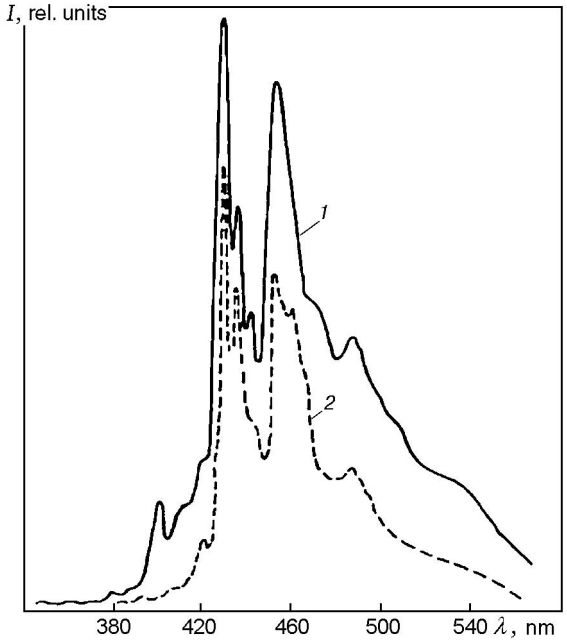

Fig. 13. Fluorescence spectra of solutions of soot extracts in iso-octane at $\lambda = 294$ (1) and 405 nm (2) [99].

The soot extracts were analyzed using IR and UV-spectroscopy. Compounds such as anthracene, anthanthrene, 1-12-benzpyrene, pyrene, coronene, and fluoranthene were identified fairly reliably. The absorption spectra also have a number of bands whose identification is hindered, i.e., the soot extracts contain mixtures of various polyaromatic compounds, whose proportion depends on the conditions of soot production.

Fluorescence spectra were taken of solutions of soot extracts in iso-octane ($\lambda = 294$ and 405 nm) (Fig. 13). In the fluorescence spectra there are intense bands with a distinct vibrational structure and the main maxima at 429, 456, 487, and 510 nm. The quantum yield of the observed fluorescence is close to 0.3. Because solution contains a mixture of polyaromatic products, it is difficult to assign the fluorescence bands to individual compounds. Nevertheless, one may state that the soot formation process involves the synthesis of PAHs that have high quantum yields of fluorescence in the blue and green regions of the spectrum.

CONCLUSIONS

The phenomenology and kinetics of soot formation, soot formation in diesel engines, the pressure effect on the soot formation process, fullerene formation during combustion, the soot formation mechanism, and simulation problems were considered.

The formation of PAHs during low-temperature combustion of propane and methane was studied experimentally. Compounds such as anthracene, anthanthrene, 1-12-benzperylene, pyrene, coronene, fluoranthene were identified. A scheme of soot formation in cool flames was proposed.

We thank Prof. B. Ya. Kolesnikov for useful discussions and D. M. Nurgozhina for the preparation of the manuscript.

This work was supported by the German Academic Exchange Service (DAAD in Germany) Foundation.

REFERENCES

1. P. A. Tesner, *Carbon Formation from Gas-Phase Hydrocarbons* [in Russian], Khimiya, Moscow (1972).
2. H. Bockhorn, F. Fetting, and H. W. Wenz, "Investigation of the formation of high molecular hydrocarbons and soot in premixed hydrocarbon–oxygen flames," *Ber. Bunsen Ges. Phys. Chem.*, **87**, 1067 (1983).
3. H. F. Calcote, "The role of ions in soot formation," in: *Abstracts of the III Int. Seminar on Flame Structure*, Alma-Ata (1989).
4. P. A. Tesner. "Soot formation during combustion," *Combust., Expl., Shock Waves*, **15**, No. 2. 111–119 (1979).
5. B. S. Haynes and H. Gg. Wagner, "Soot formation," *Prog. Energy Combust. Sci.*, **7**, 229–273 (1981).
6. H. Gg. Wagner "Soot formation in combustion," in: 17*th Symp.* (*Int.*) *on Combustion*, Combustion Inst., Pittsburgh (1979), pp. 3–19.
7. S. C. Graham, "The collisional growth of soot particles at high temperatures," in: 16*th Symp.* (*Int.*) *on Combustion*, Combustion Inst., Pittsburgh (1977), pp. 663–669.
8. K. H. Homann and H. G. Wagner, "Some aspects of soot formation," in: J. Ray Bowen (ed.), *Dynamics of Exothermicity*, Combust. Sci. and Technol. Book Series, Vol. 2, Gordon and Breach (1996), pp. 151–184.
9. I. Glassman, "Soot formation in combustion processes," in: 22*nd Symp.* (*Int*). *on Combustion*, Combustion Inst., Pittsburgh (1988), pp. 295–311.
10. J. B. Howard, "Carbon addition and oxidation reactions in heterogeneous combustion and soot formation," in: 23*rd Symp.* (*Int.*) *on Combustion*, Combustion Inst., Pittsburgh (1991), pp. 1107–1127.
11. H. Bockhorn (ed.), *Soot Formation in Combustion, Round Table Discussion*, Springer Verlag, Heidelberg (1991).
12. M. Bonig, C. Feldermann, H. Jander, et al., "Soot formation in premixed C_2H_2 flat flames at elevated pressure," in: 23*rd Symp.* (*Int.*) *on Combustion*, Combustion Inst., Pittsburgh (1991), p. 1581.
13. M. Frenklach, D. W. Clary, W. C. Gardiner, and S. E. Stein, "Effect of fuel structure on pathways to soot," in: 21*st Symp.* (*Int.*) *on Combustion*, Combustion Inst., Pittsburgh (1986), p. 67.
14. I. M. Khan, "Formation and combustion of carbon in a diesel engine," *Inst. Mech. Eng. Proc.*, **184**, Part 35, 36–43 (1969).
15. N. A. Henein, "Analysis of pollutant formation and control and fuel economy in diesel engines," *Prog. Energy Combust. Sci.*, Vol. 1, 165–207 (1976).
16. N. Petereit, *Untersuchung des Russwachstums in orgemischten atmospharischen Ethen-Flammen*, Dissertation, Gettingen (1992).
17. J. Warnatz, U. Mass, and R. W. Dibble, *Combustion: Physical and Chemical Fundamentals, Modeling and Simulation, Experiments, Pollutant Formation*, Springer, Berlin–New York (2001).
18. H. Böhm, M.Bönig, C. Felderman, et al., "Pressure dependence of formation of soot and PAH in premixed flames," in: H. Bockhorn (ed.), *Soot Formation in Combustion*, Springer Series in Chemical Physics, Vol. 59, Springer Verlag, Berlin (1994), pp. 145–164.
19. H. W. Kroto, J. R. Heath, S. C. O'Brien, et al., "C_{60}: Buckminsterfullerene," *Nature*, **318**, 162–163 (1985).
20. P. Gerhardt, S. Loffler, and K. H. Homann, "The formation of polyhedral carbon ions in fuel-rich acetylene and benzene flames," in: 22*nd Symp.* (*Int.*) *on Combustion*, Combustion Inst., Pittsburgh (1988), pp. 395–401.
21. J. B. Howard, J. T. McKinnon, Y. Makarovsky, et al., "Fullerenes C_{60} and C_{70} in flames," *Nature*, **352**, 139–141 (1991).

22. J. B. Howard, "Combustion synthesis of fullerenes and fullerenic nanomaterials for large-scale applications," in: *Abstracts of Int. Conf. on Carbon* (2004), p. 57.
23. J. B. Howard, "Fullerenes formation in flames," in: 24*nd Symp.* (*Int.*) *on on Combustion*, Combustion Inst., Pittsburgh (1992), pp. 993–946.
24. H. Richter, A. J. Labrocca, W. J. Grieco, et al., "Generation of higher fullerenes in flames," *J. Phys. Chem. B*, **101**, 1556–1560 (1997).
25. M. Frenklach and L. B. Ebert, "Comment on the proposed role of spheroidal carbon clusters in soot formation," *J. Phys. Chem.*, **92**, 561–563 (1988).
26. Q. L. Zhang, S. C. O'Brien, J. R. Heath, et al., "Reactivity of large carbon clusters: Spheroidal carbon shells and their possible relevance to the formation and morphology of soot," *J. Phys. Chem.*, **90**, 525–528 (1990).
27. K. D. Chowdhury, J. B. Howard, and J. B. Vander Sande, "Fullerenic nanostructures in flames," *J. Mater. Res.*, **11**, 341–347 (1996).
28. W. J. Grieco, A. L. Lafleur, K. C. Lafleur, et al., "Fullerenes and PAH in low-pressure premixed benzene/oxygen flames," in: 27*th Symp.* (*Int.*) *on Combustion*, Combustion Inst., Pittsburgh (1998), pp. 1669–1675.
29. D. Ugarte, "High-temperature behavior of fullerene black," *Carbon*, **32**, 1245–1248 (1994).
30. W. J. Grieco, J. B. Howard, L. C. Rainey, and J. B. Vander Sande, "Fullerenic carbon in combustion-generated soot," *Carbon*, **38**, 597–614 (2000).
31. A. L. Lafleur, J. B. Howard, K. Taghizadeh, et al., "Identification of $C_{30}H_{10}$ dicy-dopentapyrenes in flames: Correlation with corannulene and fullerene formation," *J. Phys. Chem.*, **100**, 17421–17428 (1996).
32. A. L. Lafleur, J. B. Howard, J. A. Marr, and T. Yadav, "Proposed fullerene precursor corannulene identified in flames both in the presence and absence of fullerene production," *J. Phys. Chem.*, **97**, 13539–13543 (1993).
33. C. J. Pope and J. B. Howard, "Further testing of the fullerene formation mechanism with predictions of temperature and pressure trends," in: 25*th Symp.* (*Int.*) *on Combustion, Combustion Inst.*, Pittsburgh (1994), pp. 671–678.
34. T. Baum, P. Loffler, P. Weilmunster, and K.-H. Weilmunster, "Fullerene ions and their relation to PAH and soot in low-pressure hydrocarbon flames," *Ber. Bunsenges Phys. Chem.*, **96**, 841–857 (1992).
35. M. Bachmann, W. Wiese, K.-H. Homann, "Fullerenes versus soot in benzene flames," *Combust. Flame*, **101**, 548–550 (1995).
36. J. Ahrens, R. Kovacs, E. A. Shafranovskii, and K.-H. Homann, "Online multi-photon ionization mass spectrometry applied to PAH and fullerenes in flames," *Ber. Bunsenges Phys. Chem.*, **98**, 265–268 (1994).
37. J. Ahrens, M. Bachmann, T. Baum, et al., "Fullerenes and their ions in hydrocarbon flames," *Int. J. Mass Spectrom. Ion Process.*, **138**, 133–148 (1994).
38. M. Bachmann, W. Wiese, and K.-H. Homann, "PAH and aromers: precursors of fullerenes and soot," in: 26*th Symp.* (*Int.*) *on Combustion*, Combustion Inst., Pittsburgh (1996), pp. 2259–2267.
39. A. J. Stone and D. J. Wales, "Theoretical studies of icosahedral C_{60} and some related species," *Chem. Phys. Lett.*, **128**, 501–503 (1986).
40. L. T. Scott, "Particles of fullerenes: novel syntheses, structures, and reactions," *Pure Appl. Chem.*, **68**, 291–300 (1996).
41. J. T. McKinnon, W. Bell, and R. M. Barkley, "Combustion synthesis of fullerenes," *Combust. Flame*, **88**, 102–112 (1992).
42. L. Yuan, K. Saito, C. Pan, et al., "Nanotubes from methane flames," *Chem. Phys. Lett.*, **340**, 237–241 (2001).
43. L. Yuan, K. Saito, W. Hu, and Z. Chen, "Ethylene flame synthesis of well-aligned multiwalled carbon nanotubes," *Chem. Phys. Lett.*, **346**, 23–28 (2001).
44. R. L. Vander Wal, T. M. Ticich, and V. E. Curtis, "Substrate-support interactions in metal-catalyzed carbon nanofiber growth," *Carbon*, **39**, 2277–2289 (2001).
45. R. L. Vander Wal, L. J. Hall, and G. M. Berber, "Optimization of flame synthesis for carbon nanotubes using supported catalyst," *J. Phys. Chem. B*, **106**, 13122–13132 (2002).
46. R. L. Vander Wal, "Fe-catalyzed single-walled carbon nanotube synthesis within a flame environment," *Combust. Flame*, **130**, 37–47 (2002).
47. A. V. Saveliev, W. Merchan-Merchan, and L. A. Kennedy, "Metal catalyzed synthesis of carbon nanostructures in an opposed flow methane oxygen flame," *Combust. Flame*, **135**, 27–33 (2003).
48. L. Yuan, T. Li, and K. Sano, "Synthesis of multi walled carbon nanotubes using methane/air diffusion flames," *Proc. Combust. Inst.*, **29**, 1087–1092 (2002).
49. W. Merchan-Merchan, A. V. Saveliev, and L. A. Kennedy, "High-rate flame synthesis of vertically aligned carbon nanotubes using electric field control," *Carbon*, **42**, 599–608 (2004).
50. G. W. Lee, J. Jurng, and J. Hwang, "Formation of Ni-catalyzed multiwalled carbon nanotubes and nanofibers on a substrate using an ethylene inverse diffusion flame," *Combust. Flame*, **139**, 167–175 (2004).
51. C. S. Mcneally, U. O. Koyliu, L. D. Pfefferle, and D. F. Rosner, "Soot volume fraction and temperature measurements in laminar nonpremixed flames using thermocouples," *Combust. Flame*, **109**, 701–720 (1997).

52. T. Flesch, C. McCarthy, A. Basn, et al., "A new pure diesel technology: Demonstration of ULEV emissions on a navistar diesel engine fueled with dimethyl ether," in: *Proc. of the Int. Congress and Exposition*, Detroit, Feb. 27–Mar. 2 (1995), SAE Paper 950061.
53. P. A. Tesner and S. V. Shurupov, "Some physicochemical parameters of soot formation during pyrolysis of methane and methane–benzene mixtures," *Proc. Combust. Inst.*, **25**, 653–659 (1994).
54. P. A. Tesner and S. V. Shurupov, "Some physicochemical parameters of soot formation during pyrolysis of hydrocarbons," *Combust. Sci. Technol.*, **105**, 147–161 (1995).
55. P. A. Tesner and S. V. Shurupov, "Soot formation during pyrolysis of naphthalene, anthracene, and pyrene," *Combust. Sci. Technol.*, **126**, 139–152 (1997).
56. S. V. Shurupov and P. A. Tesner, "Soot formation during isothermal pyrolysis of carbon tetrachloride and methane–carbon tetrachloride mixture," *Proc. Combust. Inst.*, **27**, 1581–1588 (1998).
57. S. V. Shurupov, "Particulate carbon formation from hydrocarbon mixtures," *Exp. Therm. Fluid Sci.*, **21**, 26–32 (2000).
58. S. V. Shurupov, "Some factors that govern particulate carbon formation during pyrolysis of hydrocarbons," *Proc. Combust. Inst.*, **28**, 2507–2514 (2000).
59. K.-H. Homman and H. G. Wagner, "Some new aspects of the mechanism of carbon formation in premixed flames," in: 11*th Symp.* (*Int.*) *on Combustion*, Combustion Inst., Pittsburgh (1967), pp. 371–379.
60. S. E. Stein and A. Fank, "High temperature stabilities of hydrocarbons," *J. Phys. Chem.*, **89**, 3714–3725 (1985).
61. J. A. Miller and C. E. Melius, "Kinetics and thermodynamic issues in the formation of aromatic compounds in flames of aliphatic fuels," *Combust. Flame*, **91**, 21–39 (1992).
62. N. M. Marinov, W. J. Pitz, and C. K. Westbrook, "The formation of aromatics and PAH's in laminar flames," in: *Joint of Meeting of the British*, German and Franch Sections (1999), p. 7.
63. C. E. Edwards and P. J. Goix, "Effect of fuel gas composition and excess air on VOC emissions from technology," *Combust. Sci. Technol.*, **116–117** (1996), p. 375.
64. DOE/PERF Burner Data. (1997).
65. P. A. Vlasov and W. Warnatz, "Kinetic simulation of soot formation by pyrolysis of various aliphatic and aromatic hydrocarbon in shock tubes," *Khim. Fiz.*, **23**, No. 10, 39–46 (2004).
66. B. A. Urmashev, T. T. Mashan, B. Ya. Kolesnikov, and Z. A. Mansurov, "Experimental and theoretical investigation of low temperature PAH and soot formation on hydrocarbon flames," in: 18*th Int. Colloquium on the Dynamics of Explosions and Reactive Systems*, Seattle (2001).
67. A. V. Krestinin, M. B. Kislov, A. V. Raevskii, et al., "On the formation mechanism of soot particles," *Kinet. Katal.*, No. 1, 102–111 (2000).
68. H. Richter and J. B. Howard, "Formation of polycyclic aromatic hydrocarbons and their growth to soot — a review of chemical reaction pathways," *Prog. Energy Combust. Sci.*, **26**, 565–608 (2000).
69. J. B. Howard, "Carbon addition and oxidation reactions in heterogeneous combustion and soot formation," *Proc. Combust. Inst.*, **23**, 1107–1127 (1990).
70. M. Frenklach, "Reaction mechanism of soot formation in flames," *J. Phys. Chem. Chem. Phys.*, **4**, 2027–2037 (2002).
71. S. J. Harris and A. M. Weiner, "A picture of soot particle inception," *Proc. Combust. Inst.*, **22**, 333–342 (1988).
72. T. G. Benish, A. L. Lafleur, K. Taghizadeh, and J. B. Howard, "C_2H_2 and PAH as soot growth reactants in premixed C_2H_4–air flames," *Proc. Combust. Inst.*, **26**, 2319–2326 (1996).
73. S. Macadam, J. M. Beer, and A. B. Hoffmann, "Soot surface growth by polycyclic aromatic hydrocarbon and acetylene addition," *ibid.*, pp. 2295–2302.
74. A. Kazakov and M. Frenklach, "On the relative contribution of acetylene and aromatics to soot particle surface growth," *Combust. Flame*, **112**, 270–274 (1998).
75. A. Ciajolo, R. Barbella, A. Tregrossi, and L. Bonfanti, "Spectroscopic and compositional signatures of PAH-loaded mixtures in the soot inception region of a premixed ethylene flame," *Proc. Combust. Inst.*, **27**, 1481–1487 (1998).
76. W. J. Grieco, J. B. Howard, L. C. Rainey, J. B. Vander Sande. "Fullerenic carbon in combustion-generated soot," *Carbon*, **38**, 597–614 (2000).
77. L. G. Blevins, R. A. Fletcher, B. A. Benner, et al., "The existence of young soot in the exhaust of inverse diffusion flames," *Proc. Combust. Inst.*, **29**, 2325–2333 (2002).
78. K.-H. Homann and H. Gg. Wagner, "Some new aspects of the mechanism of carbon formation in premixed flames," *Proc. Combust. Inst.*, **11**, 371–379 (1967).
79. H. Richter, S. Granata, W. H. Green, and J. B. Howard, "Detailed modeling of PAH and soot formation in laminar preliminary mixture benzene/oxygen/argon at low pressure flame," *Proc. Combust. Inst.*, **30**, 1397–1405 (2004).
80. H. Wang and M. Frenklach, "A detailed kinetic modeling study of aromatics formation in laminar premixed acetylene and ethylene flames," *Combust. Flame*, **110**, 173–221 (1997).
81. H. Richter, W. J. Grieco, and J. B. Howard, "Formation mechanism of polycyclic aromatic hydrocarbons and fullerenes in premixed benzene flames," *Combust. Flame*, **119**, 1–22 (1999).

82. M. Frenklach and H. Wang, "Detailed mechanism and modelling of soot particle formation, soot formation in combustion, mechanism and models," in: H. Bakhorn (ed.), *Soot Formation in Combustion*, Springer Series in Chemical Physics, Vol. 59, Springer Verlag, Berlin (1994), p. 165.
83. C. J. Pope and J. B. Howard, "Simultaneous particle and molecule modeling (SPAMM): An approach for combining sectional aerosol equations and elementary gas-phase reactions," *Aerosol Sci. Technol.*, **27**, 73–94 (1997).
84. A. Krestinin, "Polyyne model of soot formation process," *Proc. Combust. Inst.*, **27**, 1557–1563 (1998).
85. R. J. Hall, M. D. Smooke, and M. B. Colket, "Predictions of soot dynamics on opposed jet diffusion flames" in: F. L. Dryer and R. F. Sawyer (eds.), *Physical and Chemical Aspects of Combustion. A Tribute to Irvin Glassman*, in: F. L. Dryer and R. F. Sawyer (eds.), Combustion Science and Technology Book Series, Vol. 4, Gordon and Breach, Amsterdam (1997), p. 189.
86. J.-B. Donnet, R. C. Bansal, and M.-J. Wang, *Carbon Black: Science and Technology*, Second ed., Dekker, New York (1993).
87. A. L. Lafleur, K. Taghizadeh, J. B. Howard, et al., "Characterization of flame-generated C_{10} to C_{160} polycyclic aromatic hydrocarbons by atmospheric pressure chemical ionization mass spectrometry with liquid introduction via heated nebulizer interface," *J. Amer. Soc. Mass Spectrom.*, **7**, 276–286 (1996).
88. J. T. McKinnon and J. B. Howard, "The roles of PAH and acetylene in soot nucleation and growth," *Proc. Combust. Inst.*, **24**, 965–971 (1992).
89. W. J. Grieco, A. L. Lafleur, K. C. Swallow, et al., "Fullerenes and PAH in low-pressure premixed benzene/oxygen flames," *Proc. Combust. Inst.*, **27**, 1669–1675 (1998).
90. A. Goel, P. Hebgen, J. B. Vander Sande, and J. B. Howard, "Combustion synthesis of fullerenes and fullerenic nanostructures," *Carbon*, **40**, 177–182 (2002).
91. B. L. Wersborg, J. B. Howard, G. C. Williams, "Physical mechanisms in carbon formation in flames," in: 14*th Symp.* (*Int.*) *Combustion*, Combustion Inst., Pittsburgh (1973), p. 929.
92. U. Bonne, K. H. Homann, and H. Gg. Homann, "Carbon formation in premixed flames," *Proc. Combust. Inst.*, **10**, 503–512 (1965).
93. V. Ya. Shtern, *Mechanism of Gas Phase Oxidation of Hydrocarbons* [in Russian], Izd. Akad. Nauk SSSR, Moscow (1960).
94. M. D. Pogosyan, T. G. Simonyan, S. D. Arsentev, A. A. Mantashyan, *Mechanism of Heat Release and Accumulation of Radicals in Cool-Flame and High-Temperature Oxidation of Propane* [in Russian], Inst. of Theor. and Appl. Mech., Novosibirsk (1988).
95. H. Bohm, D. Hesse, H. Jander, et al., "The influence of pressure and temperature on soot formation in premixed flames," in: 22*nd Symp.* (*Int.*) *on Combustion*, Combustion Inst., Pittsburgh (1988), pp. 403–411.
96. Z. A. Mansurov, "Combustion, detonation, shock waves," in: *Proc. of the Zeldovich Memorial*, Vol. 2 (1994), pp. 51–54.
97. Z. A. Mansurov, A. A. Merkulov, V. T. Popov, et al., " Formation of ultrafine soot in methane combustion in electric field," in: *Khim. Tverd. Topliva*, No. 3, 83–86 (1994,).
98. Z. A. Mansurov, B. K. Tuleutaev, V. T. Popov, et al., "Soot formation in low-temperature combustion of methane," *Combust., Expl., Shock Waves*, **27**, No. 1, 42–45 (1991).
99. Z. A. Mansurov, "Cool sooting flames of hydrocarbons," *J. Thermal Sci.*, **10**, No. 3, 269–280 (2001).
100. Z. A. Mansurov, V. I. Pesterev, et al. "On polycyclic aromatic hydrocarbon formation in the sooty flames of methane and propane," *Arch. Combust.*, **10**, Nos. 1–4, 209–215 (1990).